Electronic Supplementary Information: Orthogonal wave superposition of wrinkled, plasma-oxidised, polydimethylsiloxane surfaces

Luca Pellegrino,[1] Sepideh Khodaparast,[1] and João T. Cabral[1]

[1]*Department of Chemical Engineering, Imperial College London, UK*

2D WRINKLING PROFILE ANALYSIS

To assess the uniformity of the topographies generated via the 2D wrinkling procedure, profiles obtained from AFM were analysed along the hills and valleys of the final surface pattern. Resulted profiles are reported for samples $(120\ \|, 6\perp)$s $(20\ \|, 10\perp)\%\epsilon_{pre}$ 20W (Fig. 1a) and $(120\ \|, 50\perp)$s $(20, 10\perp)\%\epsilon_{pre}$ 20W (Fig. 1b).

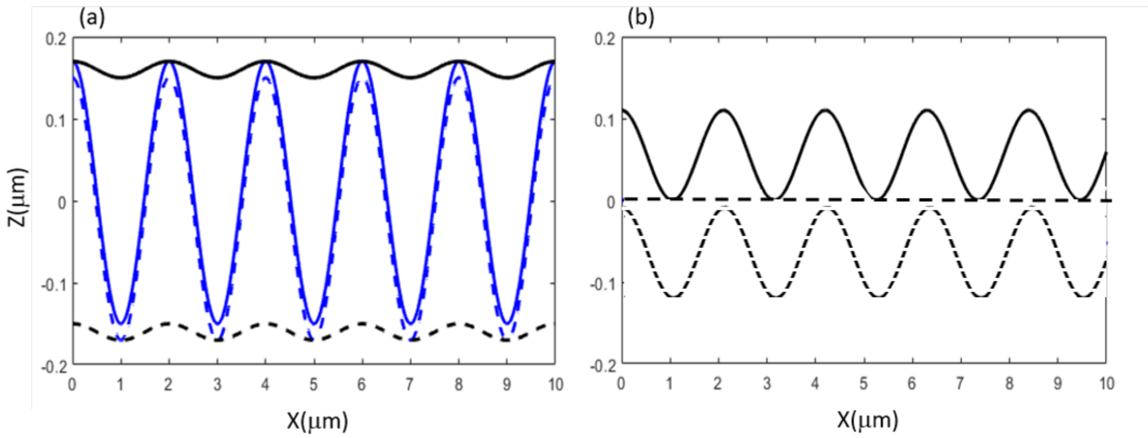

Figure 1: AFM line profiles extracted for the parallel (blue lines) and perpendicular (black lines) patterns for the: (a) $(120\ \|, 6\perp)$s $(20\ \|, 10\perp)\%\epsilon_{pre}$ 20W sample, and (b) $(120\ \|, 50\perp)$s $(20, 10\perp)\%\epsilon_{pre}$ 20W sample. The dashed lines in (a) represent the valley profiles, which are absent in (b) due to the exact superposition found in the symmetric checkerboard pattern.

As shown in Fig. S1, it is possible to distinguish between the parallel and perpendicular patterns in sample (a) due to the high mismatch in amplitudes of the corresponding waves. The sine wave profiles extracted form the hills (solid) or the valleys (dashed) are similar indicating that the perpendicular profile (black) lays on top of the hill and at the bottom of the valley of the parallel pattern with an equal amplitude value. Although similar effect is present for sample (b), it is not possible to distinguish the parallel patterns from those generated perpendicularly, due to the exact superposition of the two waves. In this sample as well, the sine waves extracted along the hills and valleys acquire identical amplitude values.

The effect of crack formation on the overall 2D pattern was investigated, see Fig. 2. Such cracks are generated by the compressive stress release generated in the direction orthogonal to the strain application. It is noticeable in Fig. 2a, that the perpendicular patters are strongly affected by the crack formation. These defects are generated during the 2D wrinkling step at the sites of the pre-existent cracks found on the parallel pattern (1D replica), which serve as stress releasing locations. The crack formation induces bulging of the mean plane of the surface before and after the crack depression, a phenomenon defined as creasing. After subtracting the creasing baseline (Fig. 2b), the resulting 'linearised' pattern shows higher amplitude of the perpendicular waves in proximity of the crack depression or valley.

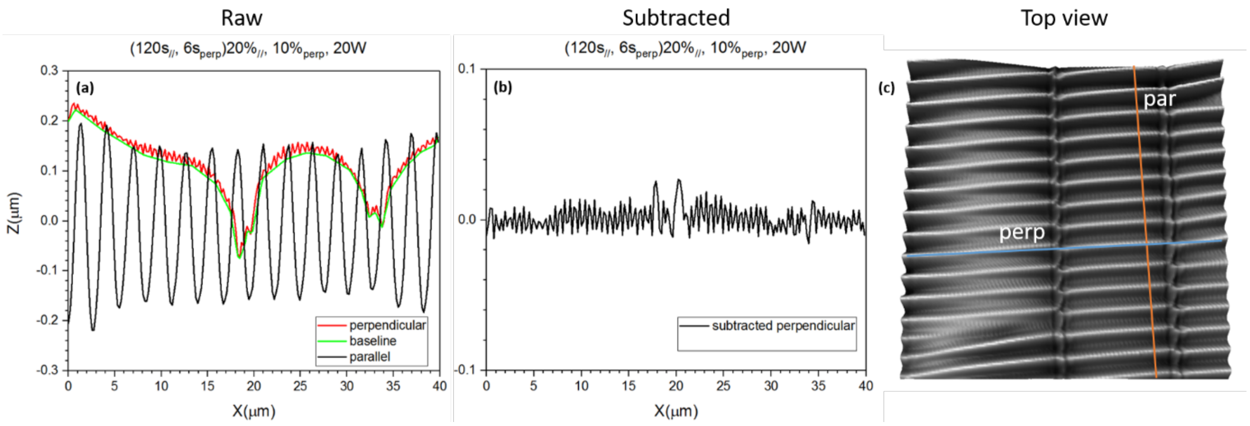

Figure 2: Effect of crack formation. (a) Total AFM line profiles extracted along the parallel (black) and perpendicular (red) wrinkling pattern for the $(120\|, 6\perp)s(20\ \|, 10\perp)\%\epsilon_{pre}$ 20W sample. The green curve represents a baseline extracted from the perpendicular pattern to remove the bulge profile generated due to crack formation. (b) 'linearised' perpendicular pattern obtained by subtracting the baseline (green curve) from the raw perpendicular profile (red curve) in (a). (c) Top view of the AFM micrograph analysed to obtain profiles presented in (a) and (b).

EFFECT OF PERPENDICULAR PRESTRAIN ON PARALLEL PATTERNS

As reported in the manuscript, the current 2D wrinkling pattern originates from the combination of two orthogonal sine waves. After the replication step, the 1D$\|$ replica is strained at 90° and subsequently plasma treated to generate a second glassy layer that forms the perpendicular wrinkling pattern after strain release. Based on previous theoretical and experimental wrinkling studies, it is well known the amplitude of the waves increases with square root of the prestrain value, while wavelength of the resulting waves decreases monotonically with the prestrain. These relationships consider a prestretch applied to a flat surface with no pre-existent wrinkling pattern.

However, our current sequential 2D wrinkling procedure involves stretching of a prepatterned surface (here the 1D$\|$ replica). Therefore, we investigated the effect of the perpendicular prestretch, applied with at 90° to the replica, with respect the first strain application (Fig. 3).

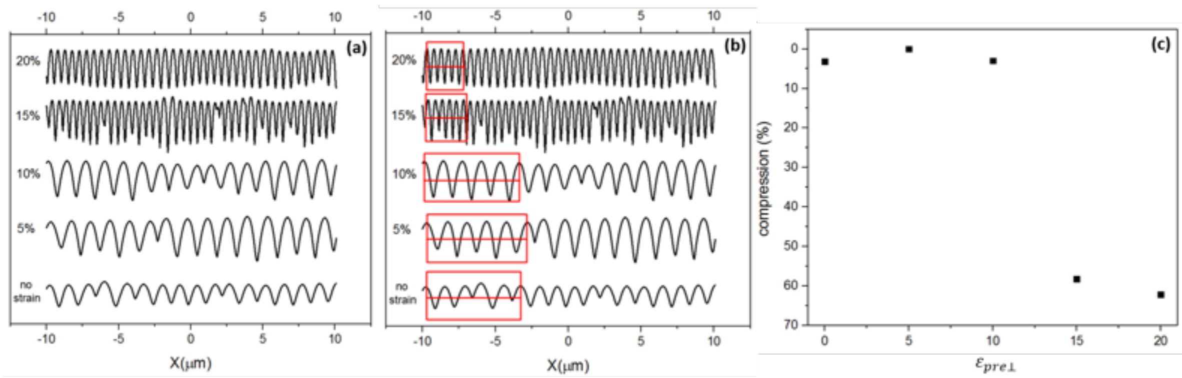

Figure 3: Effect of perpendicular prestrain on parallel patterns. (a) AFM line profiles of the 1D$\|$ replica exposed to different perpendicular prestrains ϵ_{pre}. (b) A window of 5 wavelengths was selected to analyse the lateral compression as function of the applied prestrain. (c) Quantified percentage of relative compression in the parallel wavelength at different perpendicular prestrains ϵ_{pre}.

The application of a linear prestrain along the wrinkling direction induces a lateral compression in the PDSM slab, that is clearly visible for values of prestrain above 10% (Fig. 3a,b). This compression leads to the packing of the wrinkles, that consequently induces an increase in the amplitude of the parallel waves. Starting from 15% strain, significant reduction of about 60% in the wavelength (Fig. 3c) and a total increase of about 30% in amplitude (Fig. 4) are found due to the lateral compression.

The increase in the amplitude and the decrease in wavelength are associated to the compression that the sample experiences during the application of the perpendicular strain. Such compression is orthogonal to the strain direction. The non-monotonic decrease in wavelength is not trivial to explain from the AFM data, but can be likely due to secondary relaxation phenomena happening during the strain application, such as broadening of the cracks or initial plastic deformations in the elastomer due to the higher values of prestrain. This step can be included in our sequential wrinkling procedure as an intermediate stage during the application of the orthogonal prestrain, as reported schematically in Fig. 5. It

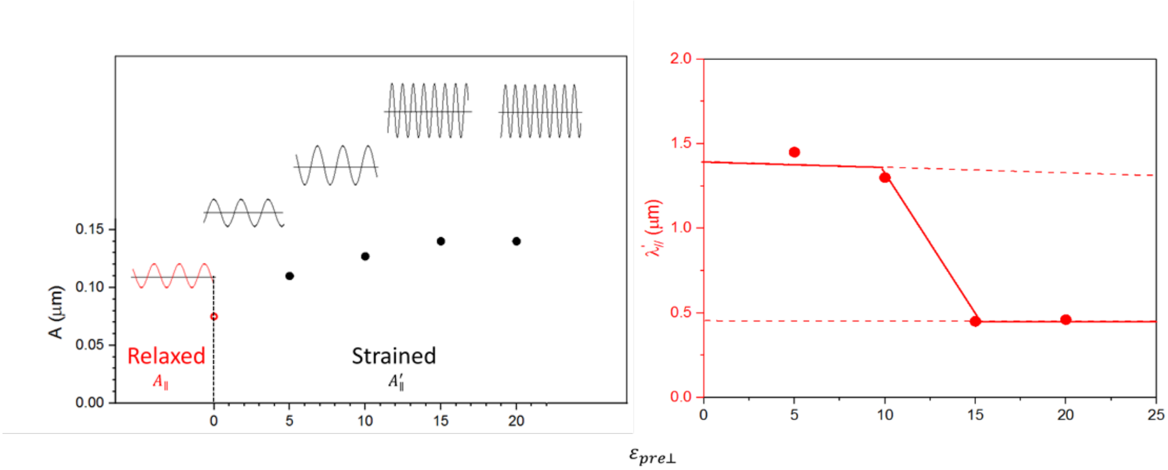

Figure 4: Amplitude (a) and wavelength (b) dependency on the perpendicular prestrain of a 1D$\|$ patterned replica. (a) The amplitude of the waves is growing with the prestrain, due to the lateral compression, until reaching a plateau at about 15% of strain. (b) The wavelength of the parallel waves remains roughly constant until reaching 10% prestrain, where it undergoes an abrupt reduction.

should be noted that for the results reported in the manuscript, the change in the wavelength due to the perpendicular prestrain application is not significant for the range of parameters used, whereas 50% increase in the amplitude of the waves is found when applying 10% of perpendicular strain to the replica.

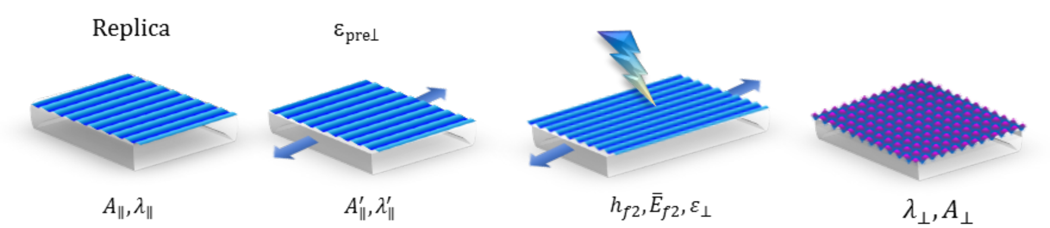

Figure 5: Application of perpendicular prestrain to the 1D$\|$ replica. The strain application generates an orthogonal compression leading to an increase in amplitude and decrease in wavelength of the parallel waves. Therefore, the pattern that undergo the secondary oxidation by plasma treatment are not the same as the replica but instead are represented by the new features noted as $A'_{\|}$ and $\lambda'_{\|}$.

Based on our findings for the effect of perpendicular prestrain on the amplitude and wavelength of the original waves, we corrected the curves describing the dependency of the pattern characteristics as functions of $\epsilon_{pre\perp}$, see Fig. 6. In general, an increase in the amplitude A is found, with respect to the no train condition, for values of prestrain starting from 5% to about 15%. Above this value no significant increase in the amplitude is observed. On the other hand, the wavelength of the waves λ remains unchanged until reaching 15% of perpendicular prestrain, where a twofold decrease is measured.

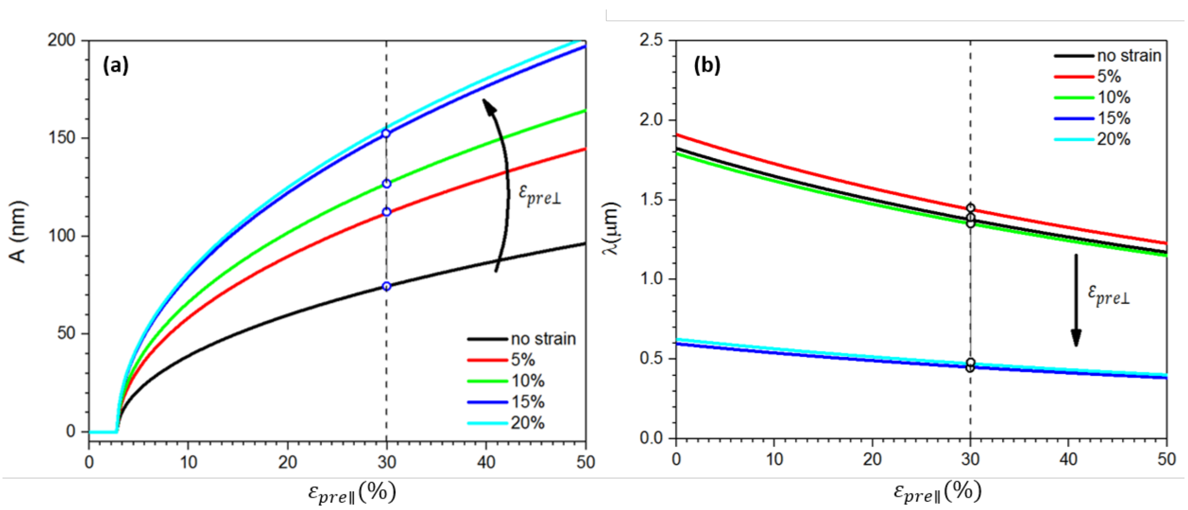

Figure 6: Amplitude and wavelength dependency on the parallel prestrain at different values of perpendicular prestrain. The solid lines represents the calculated values for A (a) and λ (b), from the wrinkling theory equations. The 1D$\|$ replica at no-strain condition (black solid curves) was fabricated with an initial 30% parallel prestrain. The blue hollow circles represent the perpendicular prestrain values $\epsilon_{pre\perp}$ applied to the 1D$\|$ replica. Other theoretical curves are obtained by using the measured values of A and λ during the application of the perpendicular strain in the equations.

ACTUAL VS NOMINAL PERPENDICULAR PRESTRAIN

In order to quantify the actual perpendicular strain applied to samples with parallel patterns, we tracked the location of dried dyed droplets sprayed on sample with first generation of waves. The difference between the relative location of the microdrops was tracked at different perpendicular prestrain values using an optical microscope. Considering the relationship between the actual and nominal perpendicular prestrain to follow:

$$\epsilon\perp_{actual} = m(1 - L/L_0), \tag{1}$$

where $(1 - L/L_0)$ is the nominal prestrain $\epsilon\perp_{nominal}$, with L being the final length and L_0 being the initial length of the replica.

Moreover, the microscopic lateral compression, orthogonal to the applied strain was measured, using similar imaging procedure. In order to investigate hysteresis effects, the deformations were recorded through cycles of extension and extension-release steps, see Fig. 7. Results of these measurements show that upto $\epsilon\perp_{nominal} = 20\%$, no significant difference between the actual and nominal prestrain values is expected.

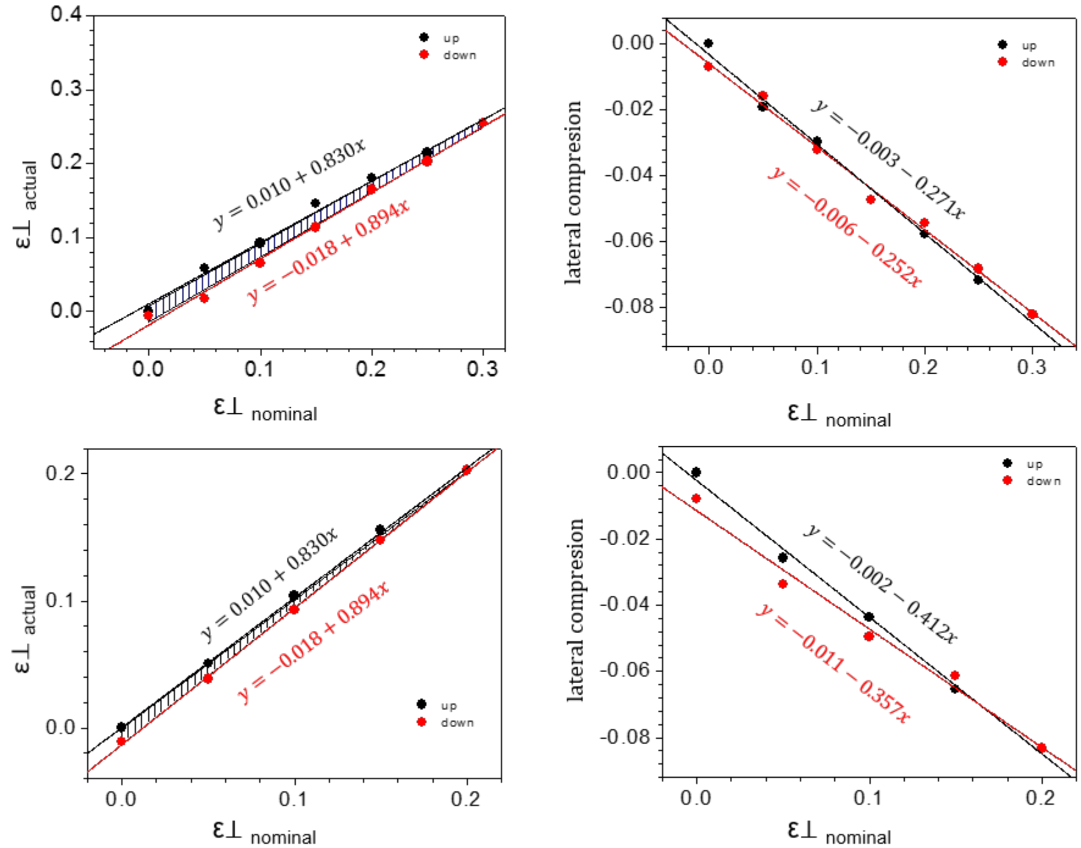

Figure 7: Measurements of actual perpendicular strain and lateral compression for a 1D$\|$ replica. (a) Stretching the sample with upto 30% of perpendicular prestrain, slight difference between the actual and nominal strain is observed, especially for $\epsilon\perp_{nominal} > 20\%$, resulting in $m = 0.8$. In the strain-release step small hysteresis effect is noticeable. Increasing the perpendicular strain, a maximum of 8% reversible lateral compression is found. (b) Similar experiment is performed by stretching the sample upto $\epsilon\perp_{nominal} = 20\%$. Unlike (a), the actual strain follows well the nominal value, thus resulting in $m = 1$. Hysteresis effects are negligible here, while the lateral compression is still present in the measurements. The hysteresis could be explained in terms of energy dissipation phenomena happening in the high deformation regime for PDMS ($\epsilon_{pre} > 20\%$).

ESTIMATED COVERAGE AND HOMOGENEITY OF 2D PATTERNS

Sequential 2D wrinkling is an efficient approach to obtain large-area checkerboard pattern compared to simultaneous 2D wrinkling process, where only herringbone can be generated. Fig. 8 shows the overall 2D patterns and crack density over an area of 400×300 μm^2 captured at four different spots of a sequentially 2D checkerboard and herringbone 2D patterned surfaces. The ratio of the crack to pattern density was estimated through mean grey value average after thresholding the micrographs to separate the areas covered by cracks from those with wrinkled patterns. For the checkerboard pattern, an overall crack density ratio of $6\% \pm 1\%$ was found, whereas this ratio was found to reach $35\% \pm 1\%$ for the herringbone pattern.

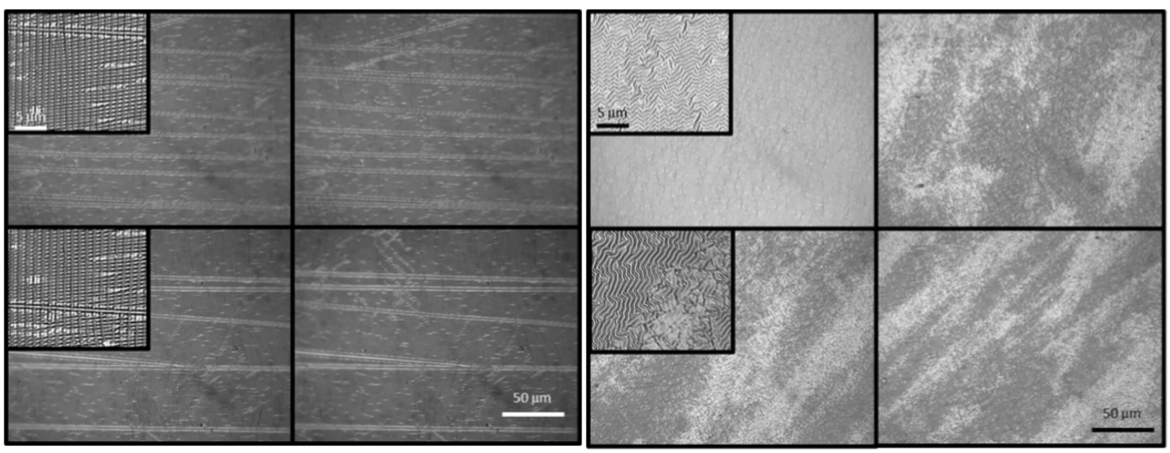

Figure 8: Analyses of the overall 2D patterns generated by sequential 2D wrinkling, using Optical microscopy over areas of 400×300 μm^2 across the sample. Left and right micrographs present checkerboard and herringbone patterns, respectively.

Although here we report a total surface area of 800×600 μm^2, it is possible to create homogeneous 2D sequential patterns over surface area of 2×2 cm^2 on a surface of a 5×5 cm^2 slab. In this estimation, only the central area of the sample is taken into account since areas close to the strain stage clamps may experience uneven stress distribution and thus generate mixed patterns. Noticeble, from the AFM analysis was possible to estimate the checkerboard to herringbone coverage (Figure 7 (a) of the manuscript) which value was found to be about 7% whereas in the sequential 2D pattern (figure 7 (b) of the manuscript) no herringbone structures were found.